ROYAL SOCIETY OF CHEMISTRY

Journal of
Materials Chemistry A

Copper- and Chloride-Mediated Synthesis and Optoelectronic Trapping of Ultra-High Aspect Ratio Palladium Nanowires

SCHOLARONE™
Manuscripts

Journal of Materials Chemistry A

ARTICLE

Copper- and chloride-mediated synthesis and optoelectronic trapping of ultra-high aspect ratio palladium nanowires

Matthew B. Lim[a], Jennifer L. Hanson[a], Leron Vandsburger[a], Paden B. Roder[a,‡], Xuezhe Zhou[a,§], Bennett E. Smith[b,‡], Fumio S. Ohuchi[a], and Peter J. Pauzauskie[*,a,c]

We present a scalable hydrothermal synthesis of one-dimensional palladium nanostructures from palladium(II) chloride precursor, mediated by the introduction of low concentrations of copper(II) ions and/or sodium chloride. Adding Cu at a molar ratio of ~1:12,500 relative to Pd increases the yield of 1D nanostructures from 10% to 90%. Furthermore, NaCl enhances 1D nanostructure growth such that high yields of long Pd nanowires (PdNWs)—featuring the highest aspect ratios yet reported for solution-grown Pd nanocrystals, with diameters of 20 nm and lengths up to 7 μm—can be achieved in a third of the time required for the synthesis with Cu alone. X-ray diffraction, electron microscopy, and X-ray photoelectron spectroscopy measurements confirm that the as-synthesized nanowires are indeed metallic crystalline Pd with a 5-fold twinned cross-section. It is hypothesized that the Cu ions scavenge oxygen to suppress etching of the twinned Pd seeds that eventually grow into elongated structures, whereas NaCl improves the solubility of $PdCl_2$ and lowers the reduction rate via formation of the $PdCl_4^{2-}$ complex, promoting diffusional growth. The high aspect ratio of the PdNWs facilitates their manipulation in an optoelectronic tweezers (OET) device, which we demonstrate as a way to enhance their applicability for catalysis and hydrogen sensing.

Introduction

Palladium nanocrystals have attracted considerable attention for their applications including hydrogen sensing and storage based on hydriding phase transformations[1–3], heterogeneous catalysis for hydrogenation, electro-oxidation of organic compounds[4–6], singlet-oxygen generation[7], and Suzuki and Heck cross-coupling reactions[8,9] which led to the Nobel Prize in Chemistry in 2010. Because the performance of Pd in such applications is highly dependent on its size, shape, and exposed facets, much research has been devoted to controlling the geometry of Pd nanocrystals during their synthesis. Additionally, considering palladium's catalytic importance, the ability to manipulate and spatially pattern Pd nanocrystals would be highly valuable, enabling one to tailor the mass transport of reactive species and the distribution of reaction products.

Toward this end, optoelectronic tweezers (OET) offers a powerful platform for large-scale patterning of nanoscale materials in solution[10–14]. This non-contact technique relies on the principle of dielectrophoresis to trap suspended particles within a well-defined area generated by shining low-power light onto a photoconductive surface sandwiched between transparent electrodes. While OET has proven useful for the patterning and separation of semiconductor and metallic nanowires[11], it requires nanostructures with high aspect ratios (L/d>100) to generate an appreciable trapping force. Hence, there is a special interest in producing Pd nanocrystals with elongated morphology. To date, several methods have been reported for the preparation of one-dimensional Pd nano-rods and wires, such as chemical vapor transport[15], electrodeposition[16,17], electron beam lithography[18], and solution-phase reduction of palladium salts[19–21].

While solution-based methods offer the most promise for scalable production, it is challenging to preferentially obtain 1D nanostructures in this manner because of palladium's face-centered cubic (FCC) structure, which provides no driving force for anisotropic growth. Polyols such as ethylene glycol are commonly used as solvents for solution-phase preparation of noble metal nanocrystals with well-defined morphologies, due to their ability to dissolve the precursor metal salts and temperature-dependent reducing power. However, product geometries are typically restricted to cuboctahedra or truncated cubes because of the rapid reduction and growth rates in polyols.[22]

In 2009, Huang and Zheng reported a hydrothermal method for the synthesis of large yields of high aspect ratio

a. Department of Materials Science and Engineering, University of Washington, Seattle, WA 98195, USA
b. Department of Chemistry, University of Washington, Seattle, WA 98195, USA
c. Physical and Computational Sciences Directorate, Pacific Northwest National Laboratory, Richland, WA 99352, USA
‡ Current address: Intel Corporation, Hillsboro, OR 97124, USA
§ Current address: Apple Inc., Cupertino, CA 95014, USA
*Email - peterpz@uw.edu
† Electronic Supplementary Information (ESI) available: Additional SEM images, XRD, NAA details, and STEM-EDS data for PdNWs. Illustration of projector-based OET manipulation of PdNWs. Video of OET manipulation of single PdNW. See DOI: 10.1039/x0xx00000x

palladium nanowires (PdNWs) using $PdCl_2$ as the metal precursor and polyvinylpyrrolidone (PVP) as both the palladium reductant and nanowire surface stabilizer[20]. They also noted the importance of NaI in promoting nanowire growth, which has since been attributed to the role of iodide as a selective capping agent for the lateral {100} facets of nanowires.[23,24] By carefully tuning the reaction time and reagent concentrations, particles with lengths up to 3 μm and diameter of ~9 nm were produced. Structurally, the nanowires have a cross-section consisting of five {111} twin planes radiating from the central <110> axis and are bounded by {100} surfaces on the sides (Fig. 1e). Unfortunately, this method as-written has not been reproducible in the present authors' hands, resulting mainly in low-aspect ratio palladium nanoparticles.

Trace impurities are known to significantly affect the solution-phase growth of metallic nanocrystals. Parts per million-level chloride impurities in the polyol synthesis of silver nanocrystals were found to inhibit the growth of irregular, twinned nanoparticles in favor of single-crystal cubes and tetrahedra.[25] Also, iodide impurities in cetyltrimethylammonium bromide (CTAB) surfactants have been shown to prevent the surfactant mediated synthesis of gold nanowires.[26] On the other hand, more recently, Tang et al. noted that the addition of trace Ag(I) or Cu(II) enhanced the yield of pentagonally twinned Pd nanorods grown in water at atmospheric pressure from $PdCl_2$, using CTAB and iodide as capping agents and ascorbic acid as the reductant.[21] While these nanorods were inferior in aspect ratio to those produced hydrothermally by Huang and Zheng, being only 100–500 nm long by 20 nm wide, the results suggest that the presence of other transition metal ions is key to producing 1D Pd nanostructures in large quantities, an idea that had not been introduced previously.

In this manuscript, we demonstrate a reproducible, high-yield route to palladium nanorods and nanowires based on the aforementioned hydrothermal method, and their utility for OET patterning. Furthermore, we show that the high yield of these 1D nanostructures is mediated by the introduction of trace Cu(II)—via soluble copper(II) acetate or copper(II) sulfate—and/or sodium chloride to the precursor solution. Nanowires produced by this approach feature a greater length and aspect ratio (up to 7 μm and 350 respectively) than any previously reported Pd nanocrystals produced by solution-phase, non-templated methods.

Experimental

Reagents

Palladium(II) chloride (99.999%), sodium iodide (≥99%), polyvinylpyrrolidone (PVP, MW=29000 or 55000), copper(II) acetate monohydrate ($Cu(OAc)_2$*H_2O, ≥98%), and sodium chloride (≥98%) were purchased from Sigma-Aldrich Corporation, USA. Copper(II) sulfate pentahydrate (≥98%) was purchased from Avantor Performance Materials, USA. Nanopure deionized water (18.2 MΩ·cm, ThermoScientific

Barnstead filtration system) was used in all experiments. All reagents were used as received without additional purification.

Synthesis

In a typical synthesis with the Cu(II) additive alone, 17.7 mg of $PdCl_2$, 300 mg of NaI, and 800 mg of PVP (MW 29000) were added to an Erlenmeyer flask with 11 mL of nanopure water. For control experiments without Cu, 12 mL of water was used. The mixture of reagents was sonicated until the NaI and PVP dissolved completely. Due to the poor solubility of $PdCl_2$ in water, the mixture was then stirred at 50°C for 10 h, and cooled back to room temperature.

For syntheses involving NaCl, 46.8 mg of NaCl was added alongside $PdCl_2$, NaI, PVP, and water in the same amounts as above, giving a $NaCl:PdCl_2$ molar ratio of 8:1. Additionally, MW 55000 PVP was substituted for MW 29000 PVP. In this case, the reagents were only stirred for 3 h at room temperature following sonication, owing to the enhanced solubility of $PdCl_2$ imparted by NaCl.

To introduce Cu(II), 1 mL of 8 μM aqueous solution prepared from $Cu(OAc)_2$·H_2O or $CuSO_4$·$5H_2O$ powder was then added dropwise to the mixture under stirring, giving 0.67 μM Cu(II) overall, or a Cu:Pd molar ratio of ~1:12500. The final precursor solution was then sealed within a 23-mL Teflon-lined steel autoclave (Parr, model #4749). To guard against contamination from other trace metals and organics, the Teflon liner was treated for 24 hours beforehand with aqua regia, prepared from a 1:3 (mol/mol) mixture of concentrated nitric and hydrochloric acids; after this time, the acid was neutralized with sodium bicarbonate and the liner was rinsed repeatedly with water. The sealed autoclave was placed in a preheated oven at 200°C for 6 h (for syntheses with Cu(II) alone) or 2 h (for syntheses with Cu(II)+NaCl or NaCl alone), after which it was removed and cooled to room temperature in ambient air. The recovered solution was diluted with isopropyl alcohol, and then repeatedly rinsed and centrifuged at 5000 rpm to precipitate the Pd particles. Samples were finally rinsed and suspended in ethanol or water before subsequent characterization. High-aspect-ratio nanowire suspensions were observed to have a dynamic opalescent texture when inverted.

Characterization

Scanning electron microscopy (SEM) images were obtained on a FEI Sirion XL30 with 10 kV accelerating voltage. Transmission electron microscopy (TEM) images with accompanying select-area electron diffraction (SAED) patterns and energy-dispersive X-ray spectra (EDS) were obtained on a FEI Tecnai G2 F20 with 200 kV accelerating voltage.

X-ray Diffraction (XRD) was performed on a Bruker D8 Discover with General Area Detector Diffraction System (GADDS) using an averaged Cu K_α radiation source ($\lambda_{K\alpha, avg}$ = 1.54184 Å) and 2θ step size 0.05°. The sample consisted of a (111) silicon wafer onto which an aqueous PdNW suspension

2 | *J. Mater. Chem. A*, 2017, **00**, 1-3

This journal is © The Royal Society of Chemistry 20xx

was evaporated, and was aligned in the system using the laser guidance system provided in the instrument.

X-ray photoelectron spectroscopy (XPS) was conducted using a PHI 5000 VersaProbe setup with Al K$_\alpha$ radiation. Samples were treated with oxygen plasma prior to analysis to etch away the existing PVP surface coating and aligned in the system using the laser guidance system provided in the instrument. Acquired spectra were deconvoluted and analyzed with PHI MultiPak software (Physical Electronics, Inc.). The energy calibrations were made against the C 1s peak (284.8 eV) of adventitious carbon as a reference. For core-level analysis of Pd, an asymmetric peak shape (Doniach-Sunjic) was used for each of the Pd subpeaks, while the oxide subpeaks were fitted with a Gaussian lineshape. FWHM values were limited to 1–1.5 eV for all peaks excepting the Pd3p$_{3/2}$, which is given a broader FWHM, as shown by Gabasch et al.[27]

Zeta potentials of the Pd particles were obtained on a Malvern Instruments Zetasizer NanoZS. The particles were dispersed dilutely in nanopure water and the zeta potential was taken as the average of 5 measurements.
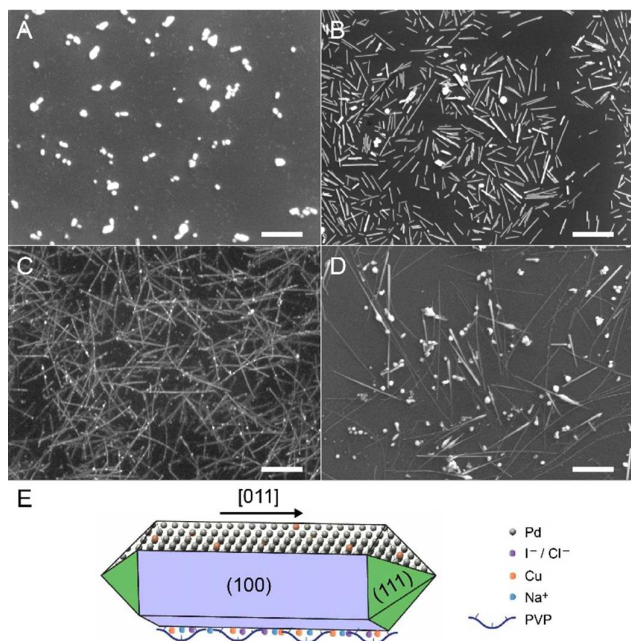
Fig. 1 SEM images of hydrothermally synthesized Pd nanoparticles (a) without additives, (b) with 0.67 μM Cu(OAc)$_2$ addition, (c) with NaCl and Cu(OAc)$_2$, and (d) with NaCl only. Scale bar = 1 μm. (e) Schematic of ideal PdNW with penta-twinned cross-section, <011> growth direction, and surface coating.

Table 1 Summary of hydrothermally synthesized 1D Pd nanostructures. Particle dimensions were measured from SEM images with sample size = 50 particles.

Additive	MW of PVP	Dwell Time @ 200°C	Average Length of 1D Structures ± SD [μm]	Yield of 1D Structures	Zeta Potential (mV)
None	29000	2 h	N/A	N/A	−40.5
None	29000	6 h	1.24 ± 0.919	~10%	−18.7
Cu(OAc)$_2$	29000	6 h	0.390 ± 0.233	~90%	−21.1
CuSO$_4$	29000	6 h	0.491 ± 0.325	~90%	−14.9
NaCl + Cu(OAc)$_2$	55000	2 h	0.935 ± 0.412	~75%	−35.3
NaCl	55000	2 h	1.83 ± 1.45	~50%	−31.2

Results and discussion

Synthetic studies

As illustrated in Fig. 1a, an exact reproduction of Huang and Zheng's synthesis,[20] with PdCl$_2$, NaI, and MW 29000 PVP in water, no prolonged incubation prior to hydrothermal treatment, and a 2 h dwell time at 200°C, only produced round blob-like particles 50–300 nm in diameter. It is worth noting that because PdCl$_2$ is poorly soluble in water, we had to add an overnight heated stirring step to dissolve it appreciably; even then, it did not always dissolve completely. Additionally, we had to increase the hydrothermal dwell time to 6 h to obtain an appreciable amount of 1D particles in the product (Fig. S1a), but their yield was only ~10%.

In contrast, adding 0.67 μM Cu(OAc)$_2$ or CuSO$_4$ to the precursor solution while maintaining the dwell time at 6 h dramatically increased the yield of 1D particles to ~90% (Fig. 1b, Fig. S1b). However, they are much shorter than those made without additives (Table 1). Both of these observations are consistent with the aforementioned report of Tang et al.,[21] who used a similarly small concentration of Cu(II) (19 μM) via CuSO$_4$. They hypothesized that Cu(II) was reduced to Cu nanoparticles, which tend to form twinned structures and could therefore serve as a template for twinned Pd nanorods. While this is a plausible explanation for their system, given the ability of ascorbic acid to reduce Cu(II) in addition to Pd(II) at elevated temperature, it is unlikely for our system due to the weaker reducing power of PVP. In fact, Gasparotto et al. found that PVP adsorbed on crystalline Pt electrodes does not begin to be oxidized until ~0.4 V vs. RHE, which is higher than the standard reduction potential of Cu (+0.34 V, Cu^{2+} + 2e$^-$ = Cu), implying that PVP cannot spontaneously reduce Cu(II) ions.[28]

Rather, we believe that Cu protects twinned Pd nuclei by acting as a sacrificial target for oxidation by O$_2$ (from ambient air) dissolved within the precursor solution. Left unchecked, the dissolved O$_2$ works in tandem with halide ions, particularly Cl$^-$, to re-oxidize the nascent metallic Pd crystals back to soluble metal–halide complexes. Since high-energy crystal

This journal is © The Royal Society of Chemistry 20xx

J. Mater. Chem. A, 2017, **00**, 1-3 | **3**

facets and defect zones are especially susceptible to this oxidative etching, the formation and growth of pentagonally twinned Pd seeds into nanowires will be greatly suppressed, as has been experimentally verified for polyol synthesis of Pd nanostructures from Na_2PdCl_4.[29] Although our introduction of $Cu(OAc)_2$ may seem counterintuitive as +2 is generally the highest oxidation state of Cu, and PVP is unlikely to reduce Cu(II) as previously stated, we speculate instead that the excess iodide in the system reduces Cu^{2+} to CuI, which can then be oxidized back to CuO by the dissolved oxygen.[30] Incidentally, for the synthesis of Ag nanowires in ethylene glycol, which also reduces Cu *in situ*, it has been shown that Cu(I) and Cu(II) salts have near-identical effectiveness in scavenging oxygen and promoting nanowire growth.[31] While Huang and Zheng's report on hydrothermal PdNW synthesis[20] does not mention the addition of Cu species, it is possible that the deionized water used by the authors contained trace Cu from the corrosion of copper pipes, thereby promoting the growth of nanowires.

Our nuclei protection hypothesis is not only corroborated by the higher yield of 1D Pd nanostructures with Cu(II), but also by their shorter average length compared to those obtained without additives. The Cu(II) species enable a higher concentration of Pd nuclei to form, particularly the penta-twinned seeds for rods and wires, which in turn restricts the extent of diffusional growth.

We also sought to address the problem of inconsistent and incomplete dissolution of $PdCl_2$ in the precursor mixture. This would have an unpredictable effect on reagent ratios, particularly the ratio of PVP to Pd precursor, which is known to heavily affect the product morphology.[20,32] We therefore introduced NaCl, which enables formation of the complex $PdCl_4^{2-}$ anion that lowers the energy of interaction with water molecules so more palladium can be solvated.[33] Indeed, when NaCl was added in an 8:1 molar ratio relative to $PdCl_2$, no residual solid was observed in the precursor mixture following sonication and 3 h of room-temperature stirring. This eliminated the need for prolonged, heated mixing prior to hydrothermal treatment. Another advantage of NaCl is that $PdCl_4^{2-}$ has a lower redox potential than Pd^{2+} alone (+0.59 V versus +0.95 V), offering a slower reduction pathway that would limit the number of nuclei and favor diffusional growth. Again in line with expectations, NaCl gave high yields of PdNWs, significantly longer than those obtained with Cu(II) alone, with only 2 h of heating at 200°C rather than 6 h (Fig. 1c, Table 1). The time savings and high aspect ratio of the PdNWs from this processes hold great promise for large-scale manufacture and OET applications.

Two surprising observations were noted with the NaCl-mediated approach, which we believe are related. The first is that we had to use larger PVP (MW 55000) to attain a high yield of nanowires; using MW 29000 PVP gave a mixture of nanowires and nanoparticles in similar proportions to the sample made without any additives (Fig. S1c). Second, even when Cu(II) species were omitted altogether, good yields of long nanowires were obtained (Fig. 1d, Table 1), considerably better than the yield from the 6 h syntheses with no additives.

This is surprising considering the excess of Cl^- in the system with NaCl, which would conceivably exacerbate oxidative etching of twinned seeds in the absence of any scavenger. A similar phenomenon has been reported for the aqueous, ascorbic acid-mediated synthesis of Pd nanoparticles with a large excess of Cl^-, where increasing the Cl^- concentration increased the size and fraction of pentagonal nanorods in the product.[34] The proposed explanation is that the extra Cl^- lowers the reduction rate by hindering contact between the Pd precursor and reducing agent, and also lowers the etch rate by obstructing O_2 from the Pd seeds. Going back to the first observation, it has also been shown that in the reduction of Na_2PdCl_4 by PVP, the conversion percentage to Pd decreases with increasing molecular weight of PVP.[32] Thus, we believe that the slower reduction in this system has a stronger effect on the product than oxidative etching. Nevertheless, it is worth noting that the nanowire yield is even better with the co-addition of $Cu(OAc)_2$ (75% vs. 50%), suggesting that oxidative etching still plays a minor role. Also, the nanowires produced with the co-addition of $Cu(OAc)_2$ are shorter on average than those produced with NaCl alone, again consistent with our hypothesis that Cu protects twinned seeds.

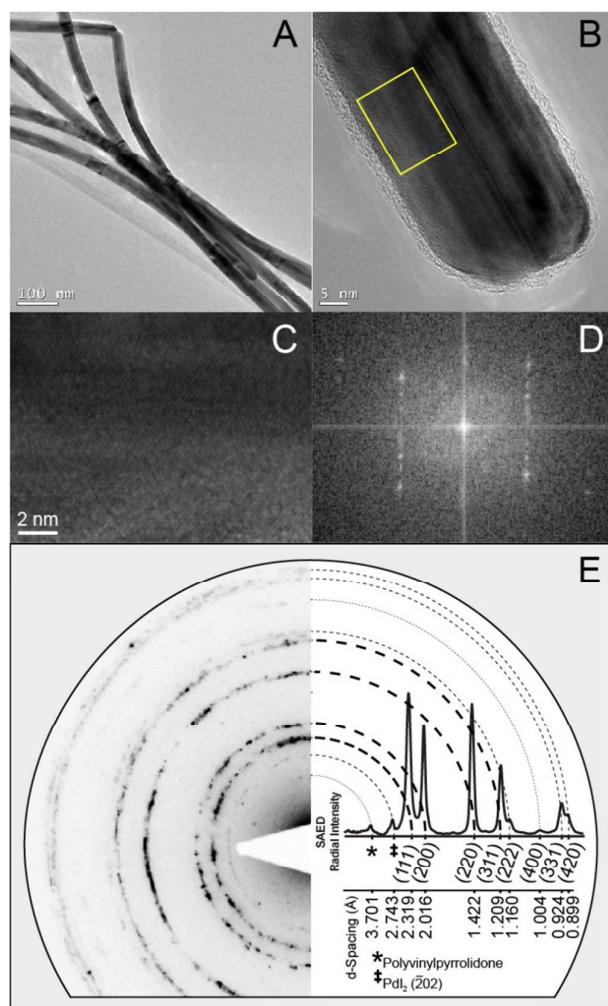Subsequent characterizations of our PdNWs in this report focus on the samples synthesized with $Cu(OAc)_2$ alone.

Characterization of Cu-mediated PdNWs

XRD, using Cu Kα radiation (λ ~ 1.54 Å), confirmed the crystallinity of the PdNWs (Fig. S2), with the diffraction peaks at 2θ = 40.1°, 46.7°, 68.1°, 82.1°, and 86.6° originating from the (111), (200), (220), (113), and (222) planes of FCC Pd respectively (JCPDS card #05-0681). According to the JCPDS card, the respective intensity values of these peaks, normalized to that of the (111) peak, are 1:0.42:0.25:0.24:0.08, while our experimental intensities follow the ratio 1:0.23:0.076:0.078:0.045 which is consistent with the nanowires' high aspect ratio. In particular, the intensity ratio between the (111) and (200) peaks is 83% higher, and the intensity ratio between the (200) and (220) peaks is 80% higher, compared to the JCPDS card. This indicates that the PdNWs are mainly bounded by {111} and {100} facets, as expected from the pentagonal wire geometry (Fig. 1e). In addition to the Pd diffraction peaks, the sharp peaks at 2θ = 28.4° and 58.9° come from the (111) and (222) planes, respectively, of the (111)-oriented silicon wafer on which the PdNWs were deposited. (Although (222) is theoretically a basis-forbidden reflection for Si, it has been observed experimentally due to the phenomenon of multiple diffraction which can make a forbidden reflection visible depending on the sample's in-plane orientation.[35])

Bright-field TEM provided evidence of the pentagonally twinned nature of the PdNWs (Fig. 2). At high magnification of a single nanowire, lattice fringes are visible with a distinctive Moiré pattern and FFT in one particular area (Fig. 2b–d), which can be interpreted in the context of a chain-like structure of five twinned tetrahedral crystals bound by {111} facets and arranged about the <011> axis. Specifically, these features

4 | *J. Mater. Chem. A*, 2017, **00**, 1-3
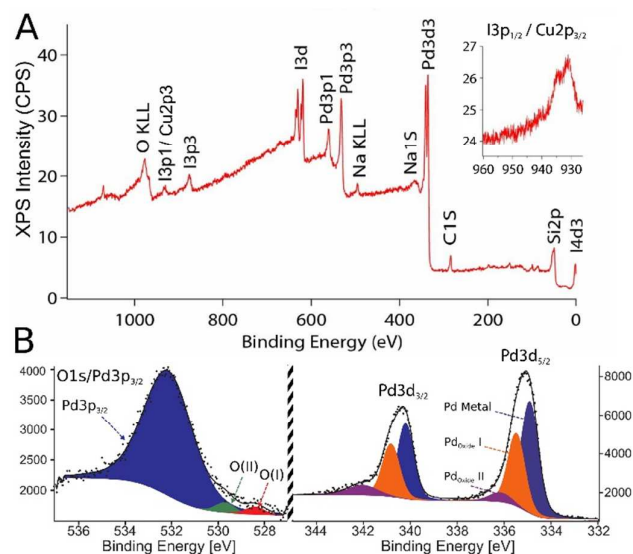
This journal is © The Royal Society of Chemistry 20xx

arise from the overlapping of the [100] and [112] zone axes when the electron beam is oriented perpendicular to one of the <011> lateral edges and its opposing {100} face. In support of this claim, a well-defined dark line appears along the middle of nanowire in Fig. 2b, corresponding to the aforementioned lateral edge. Additionally, the strong and complex contrasts observed on individual nanowires at both high and low magnification suggest numerous internal strains and defects, which are expected due to the intrinsic 7.4° angular gap of a theoretical structure of five twinned {111} tetrahedra in the FCC system. Similar FFT and contrast features have been reported for pentagonally twinned nanowires and nanorods of silver, another FCC metal.[36–38]

The peak at 3.67 Å likely originates from the PVP polymer surface coating owing to its broad shape, the sharply increasing background signal (subtracted out in Fig. 2e) for d-spacings > 2.5 Å (2θ < 36°), and the presence of a peak around a similar d-spacing in previous XRD studies of PVP.[40–42] Consistent with this hypothesis, a thin (~1 nm) amorphous layer is observed to surround the nanowire in Fig. 2b. Given that both PVP and PdI_2 would only be present at the nanowire surfaces, they would not appear in the XRD pattern due to the µm-scale penetration depth of X-rays versus the nm-scale penetration depth of electrons. Furthermore, the presence of iodide on the surface is consistent with the negative zeta potential measurements on all of our samples (Table 1), considering that PVP is a neutral polymer.[43]

Fig. 2 Bright field TEM images of (a) an aggregate of PdNWs; (b) a single PdNW. (c) Enlarged and rotated image of area outlined in (b), showing lattice fringes and moiré pattern. (d) FFT of (c). (e) Background-subtracted SAED pattern (left) with integrated intensities (right) of a cluster of PdNWs.

Fig. 3 (a) XPS survey spectrum of oxygen plasma-treated PdNW dispersion on Si substrate. $I3p_{1/2}$ binding energy at 932 eV overlaps with potential $Cu2p_{3/2}$ peak (inset). (b) High-resolution XPS spectrum of Pd3p (left) and Pd3d (right) regions with deconvoluted peaks.

SAED of a cluster of nanowires agreed with XRD and bright-field TEM on the FCC nature of the nanowires, but showed additional peaks at 2.72 and 3.67 Å d-spacing (Fig. 2e). The first of these peaks matches the d-spacing of the ($\bar{2}02$) planes of PdI_2, a phase that could form from surface iodide remnants.[39]

XPS was performed to provide chemical information for the nanowires' surface composition (Fig. 3). PdNW samples were treated with oxygen plasma to expose the metallic surface, removing the PVP polymer coating. Carbon (C1s 284 eV), sodium (Na1s 1070.5 eV), iodine ($I3p_{3/2}$ 876 eV), and palladium ($Pd3d_{5/2}$ 335, $Pd3d_{3/2}$ 340, $Pd3p_{3/2}$ 532.5, $Pd3p_{1/2}$ 561 eV) peaks are present in the spectra. Partial oxidation can be seen through double peaks for metallic and oxidized state of the iodine $I3d_{5/2}$ (619, 623 eV) and $I3d_{3/2}$ (630.5, 635 eV). An additional silicon substrate peak is visible as well (Si2p).

The presence of metallic Cu is difficult to ascertain from XPS, as the potential $Cu2p_{3/2}$ peak (expected 932 eV)[44] overlaps directly with the iodine $I3p_{1/2}$ line (Fig. 3a, inset). The shoulder at 935 eV and tail toward higher binding energy does suggest the presence of CuO, though it cannot be determined whether it was part of the nanowire as-formed, or simply developed upon exposure to air. Complementary neutron activation analysis (NAA) data confirms the presence of Cu in the nanowires at a concentration of ~62 ppm (Fig. S3).

This journal is © The Royal Society of Chemistry 20xx

J. Mater. Chem. A, 2017, 00, 1-3 | 5

Additionally, energy-dispersive X-ray spectroscopy (EDS) mapping of a PdNW in the TEM shows Cu throughout the wire with potential enrichment along its edge, whereas no Cu was detected in a background EDS spectrum of the bare SiO_2 support film of the TEM grid (Fig. S4).

High resolution analysis of the Pd3d and Pd3p peaks (Fig. 3b) suggests that the Pd present in the XPS-analyzed wires is metallic with a Pd_5O_4 monolayer film. The deconvoluted spectrum for $Pd3p_{3/2}$ was fitted to have one metal and two oxidized peak contributions, arising from the overlap of the Pd and O1s peaks. The Pd^0 peak is the largest component of the XPS signal at this energy, indicating a thin oxide film. In addition, the area ratio of the O(I) and O(II) component peaks is approximately unity (1.1–1.3). This is in line with the Pd_5O_4 surface 2D oxide phase, which has been previously reported for annealing of Pd (111) at intermediate temperatures (< 800 K).[27,45,46] The Pd3d signal is also consistent with the presence of Pd_5O_4, as the $3d_{5/2}$ and $3d_{3/2}$ peaks, offset by approximately 5.5–6 eV, can each be deconvoluted into a metal and two oxide subpeaks, following the reasoning that the Pd has two oxidation states in the film. The subpeak positions for the $3d_{5/2}$ level in particular agree with the analysis of Lundgren et al. for Pd_5O_4, the metallic Pd^0 peak being at 334.9 eV, and subsequent oxide peaks placed at 335.5 eV, and 336.2 eV.[46] For $Pd3d_{3/2}$, the Pd^0 peak is at 340.2 eV, with oxide peaks at 340.8 eV and 342.0 eV. As a side note, the energies of the fitted metallic peaks in our Pd3d spectra match those of pure bulk Pd, ruling out the presence of bimetallic PdCu species, which exhibit a slightly higher Pd3d binding energy than pure Pd due to the transfer of valence electrons from Pd to Cu.[47]

We emphasize that the presence of the palladium oxide is attributed to the oxygen plasma treatment prior to XPS, rather than to oxidation during synthesis, considering that Pd films do not oxidize spontaneously in ambient conditions.[48,49] Additionally, while to our knowledge no studies have been performed on the oxidation of polycrystalline Pd in oxygen plasma, Pd (100) surfaces have been shown to oxidize gradually to bulk PdO under oxygen plasma treatment, with accompanying broadening of the $Pd3p_{3/2}$ and $Pd3d_{5/2}$ peaks similar to our samples.[50] Furthermore, the necessity for an oxygen scavenger to grow nanowires, as demonstrated by our Cu concentration studies, speaks against the presence of a native oxide layer prior to plasma treatment.
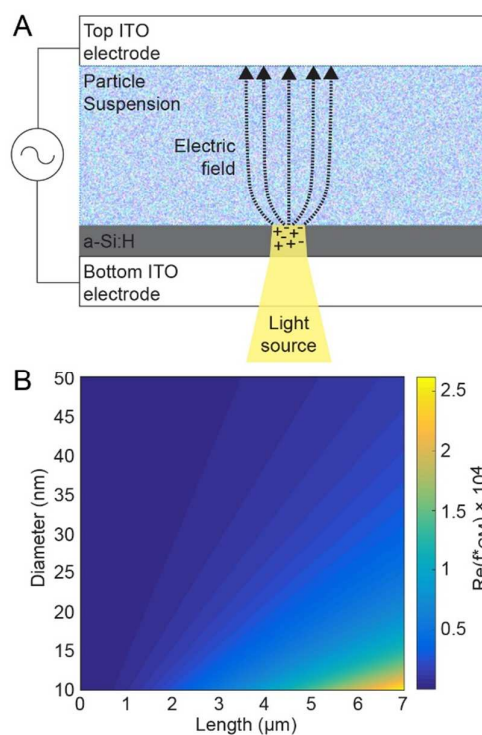

Fig. 4 (a) Schematic diagram of an OET device (ITO = indium tin oxide). (b) Calculated values of the real Clausius–Mossotti factor ($Re(f*_{CM})$) of a PdNW in water at 500 kHz for a range of particle lengths and diameters.

Optoelectronic manipulation of high-aspect ratio PdNWs

The ultra-high aspect ratio of the NaCl-enabled PdNWs also promise to provide large enough Clausius–Mossotti factors to enable trapping and patterning applications using low-cost optoelectronic tweezers (OET). OET is a non-contact, optical dielectrophoresis (DEP) based method for trapping and translating sub-millimeter particles, including one-dimensional nanostructures[11,12,51]. In a basic OET device (Fig. 4a), an aqueous dispersion of the particles of interest is placed between parallel transparent electrodes, across which an AC voltage is applied. The lower electrode is coated with a thin layer of photoconductive hydrogenated amorphous silicon (α-Si:H), such that when focused light is projected onto it, its impedance locally drops by several orders of magnitude. The resulting inhomogeneity in the electric field yields the DEP force which, if positive, drives nearby particles toward the edge of the illuminated region where the field gradient is highest.

Conventional spherical Pd nanoparticles are difficult to manipulate with OET because thermal fluctuations typically overcome the DEP force, which scales with the cube of the particle radius.[11] The real part of the Clausius–Mossotti factor, $Re[f*_{CM}]$, which determines the magnitude and direction of the DEP force, is fixed between −1/2 and 1 for a spherical particle.[52] $Re[f*_{CM}]$ can exceed 1 for elongated shapes, but even for rod-like particles, it is generally not large enough to make trapping possible at reasonable voltages. For nanorods with diameter 20 nm and length 500 nm, similar to those

6 | *J. Mater. Chem. A*, 2017, **00**, 1-3

This journal is © The Royal Society of Chemistry 20xx

reported by Tang et al.,[21] Re[f*$_{CM}$] is less than 100, assuming the medium is deionized water and the frequency of the applied field is 500 kHz. In contrast, for our highly elongated PdNWs, Re[f*$_{CM}$] is around 10^4 (Fig. 4b).
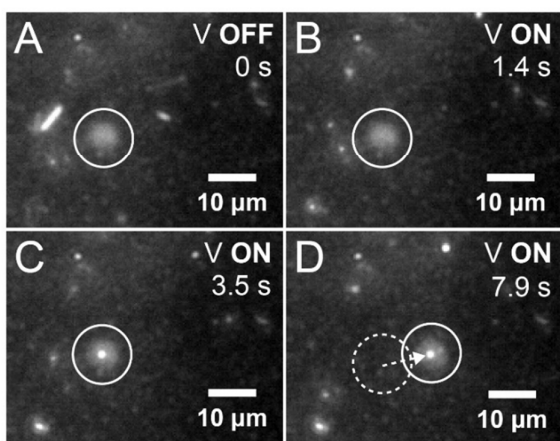
Fig. 5 Trapping and translation of a single PdNW in water with OET. Arrows indicate the location of the nanowire, and the circular outline indicates the location of the laser spot used as the trap. a) No applied bias, nanowire is in Brownian motion. b) Voltage (5 V$_{pp}$, 500 kHz) is turned on, axis of the nanowire aligns with the electric field, and it moves toward the trap. c) The nanowire has fallen into the trap. d) The nanowire follows the position of the trap as the trap is moved to the right. (Full video of the process is in Supporting Video 1.)

As visual evidence that our PdNWs can be easily trapped, Fig. 5 depicts an OET experiment with a single PdNW in water, where the a-Si:H was actuated by a helium–neon laser with wavelength 633 nm and a low optical power density of ~13 W cm^{-2}. The nanowire, approximately 6 μm long, is initially in Brownian motion. Upon applying an AC bias of 5 V peak-to-peak (V$_{pp}$) and 500 kHz, the nanowire experiences a torque that aligns its long axis parallel to the electric field (i.e., vertically within the device), causing it to appear as a dot in the microscope image. This alignment occurs because the polarizability of the nanowire's long axis is much greater than that of its short axis.[53] Within ~2 s, the nanowire falls into the nearby illuminated spot, and follows the light as it is moved.

Considering that only low-intensity light (~10 W cm^{-2}) is needed to generate significant electric field gradients, we also demonstrate that our suspended PdNWs can be trapped in bulk with an image emitted from an inexpensive digital projector (Fig. S5). This offers tremendous advantages over traditional dielectrophoretic nanowire patterning with fixed lithographically defined electrodes,[54] making it possible to form user-defined, dynamically reconfigurable arrays of nanowires using simple presentation software. Such capabilities would be particularly important for Pd considering its widespread use as a catalyst. Conceivably, reaction rates and selectivity could be optimized by controlling the arrangement of catalyst particles. Additionally, the bulk vertical alignment of PdNWs achieved with OET would create facile diffusion pathways for reagent and product species. Finally, the large-scale, solution-phase approach of OET lends itself nicely for creating Pd–carbon nanocomposites via

concurrent gelation of polymeric precursors and subsequent thermal reduction, which we have previously demonstrated with other functional nanomaterials including transition metal dichalcogenides, graphene oxide, and nanodiamonds.[55–57] This technique would allow the patterning and texturing of the PdNWs to be preserved for ex-situ uses.

Conclusions

In conclusion, palladium nanorods and nanowires have been synthesized hydrothermally by reduction of PdCl$_2$ with PVP in the presence of iodide and controlled amounts of Cu(II) salts and/or NaCl. Our analyses show that these nanostructures have the same pentagonally twinned structure as previously reported one-dimensional palladium nanocrystals, with a thin PVP/iodide surface layer. The Cu(II) ions, when present in sufficient quantities, are hypothesized to scavenge oxygen in solution that would otherwise etch the twinned Pd seeds from which nanowires grow. Furthermore, using larger molecular weight PVP, NaCl promotes growth of nanowires that are even longer than those made with the addition of Cu alone, with nanowire yield remaining high even in the absence of Cu species. This result is attributed to the slower reduction kinetics imparted by PdCl$_4^{2-}$, excess Cl$^-$, and larger PVP. Knowledge of these critical roles, which have not been elucidated previously, will facilitate large-scale, shape-controlled production of palladium nanocrystals, which is significant given their myriad applications. As one use case, we show that the high aspect ratio of our palladium nanowires makes them uniquely suited to solution-phase manipulation via optoelectronic tweezers, offering a simple means to create customizable arrays of nanowires for applications in heterogeneous catalysis.

Conflicts of interest

There are no conflicts of interest to declare.

Acknowledgements

Notes and references

1 F. Favier, E. C. Walter, M. P. Zach, T. Benter and R. M. Penner, *Science*, 2001, **293**, 2227–2231.

2 R. Griessen, N. Strohfeldt and H. Giessen, *Nat. Mater.*, 2016, **15**, 311–317.

3 L. Schlapbach and A. Züttel, *Nature*, 2001, **414**, 353–358.

4 L. D'Souza, M. Noeske, R. M. Richards and U. Kortz, *Appl. Catal. Gen.*, 2013, **453**, 262–271.

5 W. Hong, J. Wang and E. Wang, *Int. J. Hydrog. Energy*, 2014, **39**, 3226–3230.

6 H. Miyake, T. Okada, G. Samjeské and M. Osawa, *Phys. Chem. Chem. Phys.*, 2008, **10**, 3662–3669.

7 R. Long, K. Mao, X. Ye, W. Yan, Y. Huang, J. Wang, Y. Fu, X. Wang, X. Wu, Y. Xie and Y. Xiong, *J. Am. Chem. Soc.*, 2013, **135**, 3200–3207.

8 N. Miyaura, K. Yamada and A. Suzuki, *Tetrahedron Lett.*, 1979, **20**, 3437–3440.

9 R. F. Heck and J. P. Nolley, *J. Org. Chem.*, 1972, **37**, 2320–2322.

10 P. Y. Chiou, A. T. Ohta and M. C. Wu, *Nature*, 2005, **436**, 370–372.

11 A. Jamshidi, P. J. Pauzauskie, P. J. Schuck, A. T. Ohta, P.-Y. Chiou, J. Chou, P. Yang and M. C. Wu, *Nat. Photonics*, 2008, **2**, 86–89.

12 P. J. Pauzauskie, A. Jamshidi, J. K. Valley, J. H. S. Jr and M. C. Wu, *Appl. Phys. Lett.*, 2009, **95**, 113104.

13 A. Jamshidi, S. L. Neale, K. Yu, P. J. Pauzauskie, P. J. Schuck, J. K. Valley, H.-Y. Hsu, A. T. Ohta and M. C. Wu, *Nano Lett.*, 2009, **9**, 2921–2925.

14 W. Liang, N. Liu, Z. Dong, L. Liu, J. D. Mai, G.-B. Lee and W. J. Li, *Sens. Actuators Phys.*, 2013, **193**, 103–111.

15 Y. Yoo, I. Yoon, H. Lee, J. Ahn, J.-P. Ahn and B. Kim, *ACS Nano*, 2010, **4**, 2919–2927.

16 A. R. Halpern, N. Nishi, J. Wen, F. Yang, C. Xiang, R. M. Penner and R. M. Corn, *Anal. Chem.*, 2009, **81**, 5585–5592.

17 C. Koenigsmann, A. C. Santulli, E. Sutter and S. S. Wong, *ACS Nano*, 2011, **5**, 7471–7487.

18 K. J. Jeon, J. M. Lee, E. Lee and W. Lee, *Nanotechnology*, 2009, **20**, 135502.

19 Y.-H. Chen, H.-H. Hung and M. H. Huang, *J. Am. Chem. Soc.*, 2009, **131**, 9114–9121.

20 X. Huang and N. Zheng, *J. Am. Chem. Soc.*, 2009, **131**, 4602–4603.

21 Y. Tang, R. E. Edelmann and S. Zou, *Nanoscale*, 2014, **6**, 5630–5633.

22 B. Lim, M. Jiang, J. Tao, P. H. C. Camargo, Y. Zhu and Y. Xia, *Adv. Funct. Mater.*, 2009, **19**, 189–200.

23 C. Wang, L. Wang, R. Long, L. Ma, L. Wang, Z. Li and Y. Xiong, *J. Mater. Chem.*, 2012, **22**, 8195–8198.

24 H. Huang, A. Ruditskiy, S.-I. Choi, L. Zhang, J. Liu, Z. Ye and Y. Xia, *ACS Appl. Mater. Interfaces*, 2017, **9**, 31203–31212.

25 B. Wiley, T. Herricks, Y. Sun and Y. Xia, *Nano Lett.*, 2004, **4**, 1733–1739.

26 D. K. Smith, N. R. Miller and B. A. Korgel, *Langmuir*, 2009, **25**, 9518–9524.

27 H. Gabasch, W. Unterberger, K. Hayek, B. Klötzer, E. Kleimenov, D. Teschner, S. Zafeiratos, M. Hävecker, A. Knop-Gericke, R. Schlögl, J. Han, F. H. Ribeiro, B. Aszalos-Kiss, T. Curtin and D. Zemlyanov, *Surf. Sci.*, 2006, **600**, 2980–2989.

28 L. H. S. Gasparotto, J. F. Gomes and G. Tremiliosi-Filho, *J. Electroanal. Chem.*, 2011, **663**, 48–51.

29 Y. Xiong, J. Chen, B. Wiley, Y. Xia, S. Aloni and Y. Yin, *J. Am. Chem. Soc.*, 2005, **127**, 7332–7333.

30 H. J. Neuburg, *Ind. Eng. Chem. Process Des. Dev.*, 1970, **9**, 285–288.

31 K. E. Korte, S. E. Skrabalak and Y. Xia, *J. Mater. Chem.*, 2008, **18**, 437–441.

32 Y. Xiong, I. Washio, J. Chen, H. Cai, Z.-Y. Li and Y. Xia, *Langmuir*, 2006, **22**, 8563–8570.

33 T. Khoperia and T. Zedginidze, *ECS Trans.*, 2008, **13**, 95–109.

34 N. Nalajala, A. Chakraborty, B. Bera and M. Neergat, *Nanotechnology*, 2016, **27**, 65603.

35 P. Zaumseil, *J. Appl. Crystallogr.*, 2015, **48**, 528–532.

36 J. Reyes-Gasga, J. L. Elechiguerra, C. Liu, A. Camacho-Bragado, J. M. Montejano-Carrizales and M. Jose Yacaman, *J. Cryst. Growth*, 2006, **286**, 162–172.

37 H. Chen, Y. Gao, H. Zhang, L. Liu, H. Yu, H. Tian, S. Xie and J. Li, *J. Phys. Chem. B*, 2004, **108**, 12038–12043.

38 H. Hofmeister, S. A. Nepijko, D. N. Ievlev, W. Schulze and G. Ertl, *J. Cryst. Growth*, 2002, **234**, 773–781.

39 L. Wang, L. Wang, E. Tan, L. Li, L. Guo and X. Han, *J. Mater. Chem.*, 2011, **21**, 2369–2373.

40 G. S. Y. Yeh, *Pure Appl. Chem.*, 1972, **31**, 65–90.

41 N. Pradal, G. Chadeyron, S. Thérias, A. Potdevin, C. V. Santilli and R. Mahiou, *Dalton Trans.*, 2013, **43**, 1072–1081.

42 J.-F. Zhu, G.-H. Tao, H.-Y. Liu, L. He, Q.-H. Sun and H.-C. Liu, *Green Chem.*, 2014, **16**, 2664–2669.

43 K. A. Huynh and K. L. Chen, *Environ. Sci. Technol.*, 2011, **45**, 5564–5571.

44 G. Ertl, R. Hierl, H. Knözinger, N. Thiele and H. P. Urbach, *Appl. Surf. Sci.*, 1980, **5**, 49–64.

45 D. Teschner, A. Pestryakov, E. Kleimenov, M. Hävecker, H. Bluhm, H. Sauer, A. Knop-Gericke and R. Schlögl, *J. Catal.*, 2005, **230**, 186–194.

46 E. Lundgren, G. Kresse, C. Klein, M. Borg, J. N. Andersen, M. De Santis, Y. Gauthier, C. Konvicka, M. Schmid and P. Varga, *Phys. Rev. Lett.*, 2002, **88**, 246103.

47 Z. Gu, Z. Xiong, F. Ren, S. Li, H. Xu, B. Yan and Y. Du, *J. Taiwan Inst. Chem. Eng.*, 2018, **83**, 32–39.

48 C. Benvenuti, P. Chiggiato, F. Cicoira, Y. L'Aminot and V. Ruzinov, *Vacuum*, 2004, **73**, 139–144.

49 B. Wang, H. Idrissi, M. Galceran, M. S. Colla, S. Turner, S. Hui, J. P. Raskin, T. Pardoen, S. Godet and D. Schryvers, *Int. J. Plast.*, 2012, **37**, 140–156.

50 J. Wang, Y. Yun and E. I. Altman, *Surf. Sci.*, 2007, **601**, 3497–3505.

51 P. J. Pauzauskie, A. Jamshidi, J. M. Zaug, S. Baker, T. Y.-J. Han, J. H. Satcher and M. C. Wu, *Adv. Optoelectron.*, 2012, **2012**, e869829.

52 M. Esseling, *Photorefractive optoelectronic tweezers and their applications*, Springer, 2015.

53 J. J. Arcenegui, P. García-Sánchez, H. Morgan and A. Ramos, *Phys. Rev. E*, 2013, **88**, 33025.

54 P. A. Smith, C. D. Nordquist, T. N. Jackson, T. S. Mayer, B. R. Martin, J. Mbindyo and T. E. Mallouk, *Appl. Phys. Lett.*, 2000, **77**, 1399–1401.

55 M. J. Crane, M. B. Lim, X. Zhou and P. J. Pauzauskie, *Microsyst. Nanoeng.*, 2017, **3**, micronano201732.

56 M. B. Lim, M. Hu, S. Manandhar, A. Sakshaug, A. Strong, L. Riley and P. J. Pauzauskie, *Carbon*, 2015, **95**, 616–624.

57 S. Manandhar, P. B. Roder, J. L. Hanson, M. Lim, B. E. Smith, A. Mann and P. J. Pauzauskie, *J. Mater. Res.*, 2014, **29**, 2905–2911.
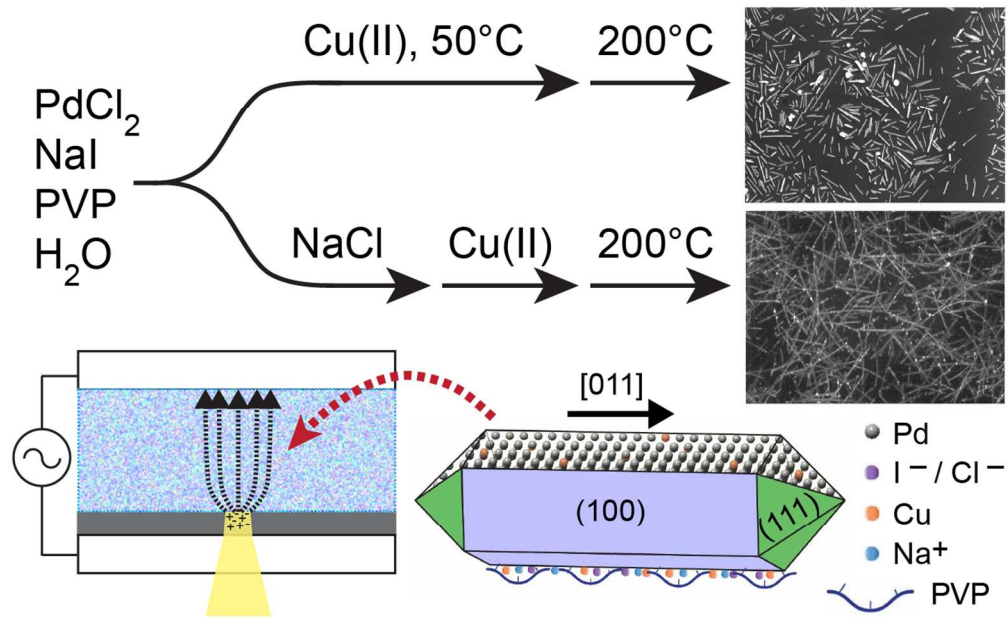
236x147mm (150 x 150 DPI)

In hydrothermal synthesis of Pd, Cu(II) and NaCl enhance yield of 1D nanostructures, which can be optically manipulated in water.